Title

Unexpected metabolic rewiring of CO2 fixation in H2-mediated materials-biology hybrids.

Journal

Proceedings of the National Academy of Sciences, 120(42)

Authors

Xie, Yongchao
Erşan, Sevcan
Guan, Xun
et al.

Publication Date

2023-10-17

DOI

10.1073/pnas.2308373120

Peer reviewed

PNAS RESEARCH ARTICLE | CHEMISTRY SUSTAINABILITY SCIENCE

Unexpected metabolic rewiring of CO_2 fixation in H_2-mediated materials–biology hybrids

Yongchao Xie[a], Sevcan Erşan[b], Xun Guan[a], Jingyu Wang[a], Jihui Sha[c], Shuangning Xu[a], James A. Wohlschlegel[c], Junyoung O. Park[b,d], and Chong Liu[a,d,1]

Edited by Thomas Mallouk, University of Pennsylvania, Philadelphia, PA; received May 18, 2023; accepted August 31, 2023

A hybrid approach combining water-splitting electrochemistry and H_2-oxidizing, CO_2-fixing microorganisms offers a viable solution for producing value-added chemicals from sunlight, water, and air. The classic wisdom without thorough examination to date assumes that the electrochemistry in such a H_2-mediated process is innocent of altering microbial behavior. Here, we report unexpected metabolic rewiring induced by water-splitting electrochemistry in H_2-oxidizing acetogenic bacterium *Sporomusa ovata* that challenges such a classic view. We found that the planktonic *S. ovata* is more efficient in utilizing reducing equivalent for ATP generation in the materials–biology hybrids than cells grown with H_2 supply, supported by our metabolomic and proteomic studies. The efficiency of utilizing reducing equivalents and fixing CO_2 into acetate has increased from less than 80% of chemoautotrophy to more than 95% under electroautotrophic conditions. These observations unravel previously underappreciated materials' impact on microbial metabolism in seemingly simply H_2-mediated charge transfer between biotic and abiotic components. Such a deeper understanding of the materials–biology interface will foster advanced design of hybrid systems for sustainable chemical transformation.

materials–biology hybrid | CO_2 fixation | metabolic rewiring | proteomics | metabolomics

The hybrid approach that integrates microbial catalysts with synthetic electrocatalysis has gained momentum in recent years for a variety of chemical transformations in the context of a sustainable future (1–6). Potentially powered by renewable energy such as solar electricity, such bioelectrochemical materials–biology hybrids have been deployed for the sustainable production of valuable commodity chemicals (7–9) and efficient remediation of environmental pollutants (10–12). In those systems, the material components serve as the sole electron donor and transduce electricity to chemical driving forces powering microbial metabolisms for desired applications under the electroautotrophic conditions (10, 13). The materials' efficient charge transfer and the microbes' synthetic versatility and selectivity synergistically coalesce at the materials–biology interactions, leading to high efficiencies and reaction throughput for challenging chemical transformations such as the fixation of CO_2 and N_2 (5, 14–19). Hence, a detailed understanding of the mutual interactions between the biotic and abiotic components (20–22) is of critical importance for the development of sustainable techniques addressing the challenges that our society is facing.

The conventional wisdom of the materials–biology hybrids assumes that while a direct physical contact of the biotic and abiotic components may affect beneficial synergies on both components (3, 6, 13), an indirect charge transfer via mediated redox couple may lead to minute if any changes on individual components' functionality. Indeed, in the research of bioelectrochemical fixation of CO_2 when H_2 generated by electrochemical proton reduction is the mediating redox species (23, 24), H_2-oxidizing chemolithotrophic *Ralstonia eutropha* (7, 25, 26), diazotrophic *Xanthobacter autotrophicus* (8, 14, 27), methanogenic *Methanosarcina barkeri* (28, 29), and acetogenic *Sporomusa ovata* (15, 30–34) were readily plugged into water-splitting electrocatalytic systems assuming no metabolomic responses and gene regulations due to the perceived indirect charge transfer in the hybrids. However, the hypothesized invariance of microbial metabolism in those H_2-mediated electroautotrophic systems has not been tested. As recent studies at the physical interface between light-absorbing semiconductors and CO_2-fixing organisms uncover unexpected material-induced metabolomic modulation (16, 35), the potential risk of understating metabolic rewiring in materials–biology hybrids with indirect charge transfer looms large, due to the absence of a thorough examination of microbial metabolism in those systems. A detailed, appropriate understanding of how microbial metabolism responds to materials' presence in H_2-mediated electroautotrophic systems will facilitate the design and development of advanced hybrids in the future.

Significance

Employing renewable electric energy to power material–microbe hybrids for chemical synthesis has emerged as a promising approach for a sustainable society. When the materials and microbes are not in physical contact with each other, it is commonly assumed that the materials component that facilitates an electron transfer mediated by redox molecules like H_2, does not serve to perturb microbial metabolism significantly. However, this study revealed that the electrochemical system can induce a fortuitous metabolic rewiring in planktonic *S. ovata* cells and an increased efficiency of utilizing provided reducing equivalents for CO_2 fixation. This observation underscores the importance of revisiting existing assumptions of materials–biology interaction and adopting a more holistic approach to understand the underlying mechanisms at material-microbe interfaces.

Author contributions: Y.X., J.O.P., and C.L. designed research; Y.X., S.E., X.G., J.W., J.S., and S.X. performed research; Y.X., S.E., J.S., J.A.W., J.O.P., and C.L. analyzed data; and Y.X. and C.L. wrote the paper.

The authors declare no competing interest.

This article is a PNAS Direct Submission.

[1]To whom correspondence may be addressed. Email: chongliu@chem.ucla.edu.

This article contains supporting information online at https://www.pnas.org/lookup/suppl/doi:10.1073/pnas.2308373120/-/DCSupplemental.

Published October 10, 2023.

We aim to rigorously test the hypothesized invariance of microbial metabolism in H_2-mediated materials-biology hybrids and hence shed more lights on the fundamental interactions between the abiotic and biotic components during the mediated indirect charge transfer (Fig. 1*A*). Built upon our previous experience (7, 14, 15, 31), the model H_2-mediated hybrid system that we aim to study includes H_2-oxidizing *S. ovata* for the fixation of CO_2 into acetic acid via the Wood–Ljungdahl pathway (36), as well as biocompatible water-splitting electrocatalysts made of cobalt–phosphorous (Co–P) alloy for hydrogen evolution reaction (HER) (Fig. 1*B*) (7). Previous studies have established a H_2-mediated delivery of reducing equivalents from the electrode to planktonic *S. ovata* under sufficiently high water-splitting current densities (31, 37). Yet, it remains unknown whether the electrochemical process(es), seemingly innocent and only responsible for H_2 generation, will perturb microbial metabolism beyond the delivery of H_2.

In this work, we report the unexpected finding that the seemingly innocent water-splitting electrocatalysis induced observable and significant metabolomic rewiring of planktonic *S. ovata* in the materials-biology hybrids of CO_2 fixation. We found a higher efficiency for microbes to utilize the generated H_2 for CO_2 fixation in the hybrid system (large than 95%), than the values observed (less than 80%) when *S. ovata* was cultured chemoautotrophically with externally supplied H_2 under otherwise the same experimental conditions (Fig. 1*A*). Metabolomic and proteomic studies comparing the electroautotrophic and chemoautotrophic cultures unraveled fortuitous metabolomic rewiring including membrane electrochemical potential regulation and enhanced proton transmembrane transport in the hybrid systems, leading to an increased adenosine triphosphate (ATP) generation and an accelerated rate of CO_2 fixation. Extracellular metabolomic data hint a process of metabolic rewiring potentially mediated by extracellular redox-active metabolites (RAMs) such as riboflavin. Our observations challenged the conventional simple picture of H_2-mediated indirect charge transfer and suggested the presence of previously underappreciated metabolic impact of inorganic electrodes on microbial catalysts. Such an advance in fundamental understanding at the materials–biology interactions heralds additional design considerations for a sustainable chemical transformation that maximizes the benefits of materials–biology hybrids.

Results

Enhanced CO_2 Fixation in H_2-Mediated Electroautotrophic Hybrid. H_2-mediated bioelectrochemical fixation of CO_2 was established in a two-chamber setup under a flowing gas environment of CO_2:N_2 (20:80, *v:v*, 6 mL min^{-1}) at 30 °C (*SI Appendix*, Fig. S1). In the cathode chamber of such setup, a biocompatible Co–P alloy HER electrocatalysts developed in our previous studies (Fig. 1*B* and *SI Appendix*, Fig. S2 *A* and *B*) (7, 14, 31, 38), composed of a P:Co weight ratio of 1:4.4 as characterized by energy-dispersive X-ray spectroscopy (*SI Appendix*, Fig. S2*C*), was applied to couple with acetogenic bacterium *S. ovata* strain H1 (DSM 2662) (39) for the reduction of CO_2 into acetic acid. Reported to yield H_2 with 100% Faradaic efficiency (38), Co–P alloy is electrocatalytically active for HER at least over 48 h based on the measured cyclic voltammograms (Fig. 1*C*) and is known to not inhibit the growth or CO_2 fixation of *S. ovata* (31). Over 48 h, a minute change of less than 0.04 V in terms of onset potentials, measured with –0.5 mA/cm^2 as the cutoff current density, suggest robust HER electrocatalysis in biological medium. The minimal medium deployed in the process does not contain any carbon substrates, except the dissolved bicarbonate ($NaHCO_3$), trace vitamin additives, and the minute amounts of cysteine as the reducing reagent (0.2 mM) for an anaerobic solution (*SI Appendix*, *Supplementary Note* 1). Two-week control experiment inoculated with *S. ovata* in CO_2:N_2 (20:80, *v:v*) but without the provision of either H_2 or electricity did not yield observable bacterial growth or acetate accumulation from CO_2 fixation (*SI Appendix*, Fig. S3). Hence, any observation of bacterial growth or acetate accumulation originates from the provision of H_2 or electricity for CO_2 fixation.

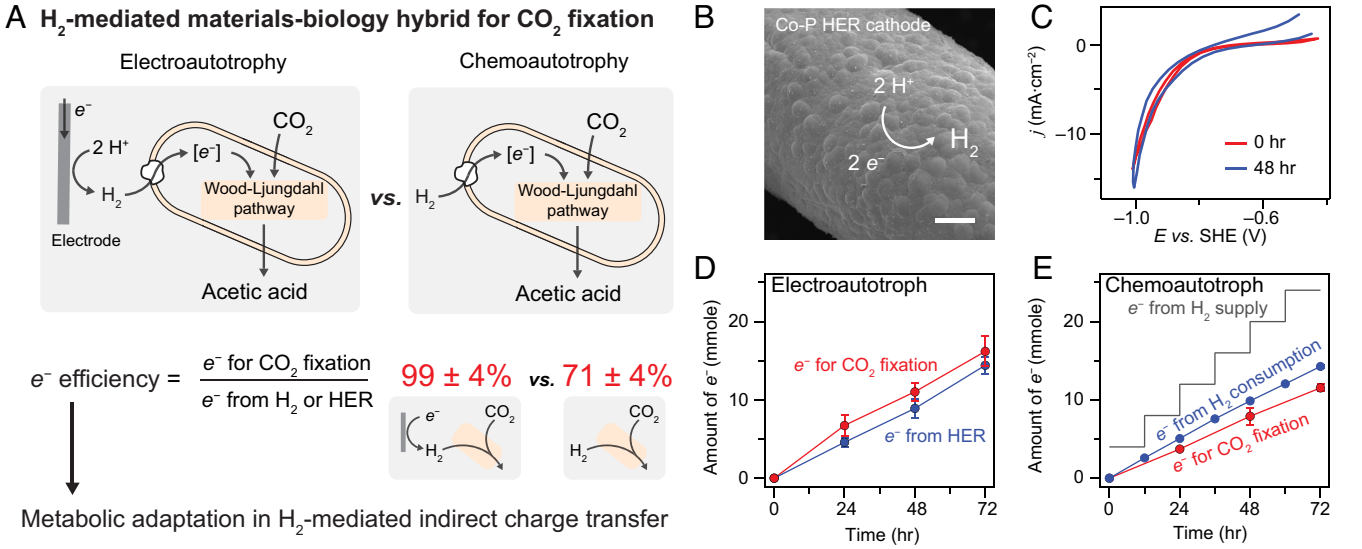

Fig. 1. Enhanced CO_2 fixation in H_2-mediated materials-biology hybrid. (*A*) Schematic comparison of *S. ovata* growth and electron efficiency (e^- efficiency) under electroautotrophic and chemoautotrophic conditions. (*B*) Scanning electron microscope image of Co–P alloy cathode for the electrocatalytic hydrogen evolution reaction (HER). (Scale bar, 10 μm.) (*C*) Current density–Voltage (*j*–V) characteristics of Co–P cathode before and after a 48-h electrolysis with a scan rate of 50 mV/s in electroautotrophic culture. SHE, standard hydrogen electrode; *iR* compensated. (*D* and *E*) The amounts of electrons consumption from respective electron donors and recovered from CO_2 fixation in *S. ovata* cultures under electroautotrophic and chemoautotrophic conditions in 72 h, before correcting for the carryover extracellular nutrients (*D* and *E*, are Entry *1* and *3* in the *SI Appendix*, Table S1, respectively). The displayed e^- efficiencies in (*A*) are the corrected ones after subtracting the carryover extracellular nutrients (*Materials and Methods*). Data represent biological triplicates ($n = 3$, same below). Error bars represent the SEM, the same below.

We report that *S. ovata* under electroautotrophic conditions in the bioelectrochemical setup is nearly 100% efficient in utilizing reducing equivalents and fixing CO_2 into acetic acid by repeated independent tests (reported as different entries in *SI Appendix*, Table S1). Chronoamperometry measurements for the materials–biology hybrid at –1.34 ± 0.10 mA/cm^2 (Entry *1*, *n* = 3, same below) equivalent to about –0.77 to –0.96 V vs. standard hydrogen electrode (SHE). In such a flowing CO_2/N_2 condition, the H_2 supply rate is 2.40 ± 0.19 millimole per day (mmole d^{-1}), equivalent to an e^- supply rate of 4.80 ± 0.37 mmole d^{-1}, while the acetate is the almost exclusive soluble organic end product and accumulation rate of acetate was determined as 0.67 ± 0.08 mmole d^{-1} based on the measurement of ^{1}H NMR spectroscopy (Entry *1* in *SI Appendix*, Table S1). Such an observed level of acetate production rate is at least comparable to our previous report (31) and other reported bioelectrochemical systems deploying acetogens for CO_2 fixation (*SI Appendix*, Table S2). In two independent tests, the apparent electron efficiency $\eta_{app,electro}$, or the apparent Faradaic efficiency that describes the percentage of electrons contributing to CO_2 reduction into acetic acid, was calculated to be 112 ± 6% and 110 ± 9% (Entry *1* and *2* in *SI Appendix*, Table S1, respectively), based on the trajectory of acetate accumulation sampled every 24 h (Fig. 1*D*). The higher-than-100% $\eta_{app,electro}$ is proposed to originate from the residual extracellular oxidizable organics carried over during bacterial inoculation (40), since the chemical oxygen demand (COD) of the extracellular component of the *S. ovata* inoculum at the beginning of experiments was measured to be 1.99 ± 0.85 mmole of electron equivalents. Accounting the contribution of residual extracellular oxidizable organics (*SI Appendix*, Fig. S4), the corrected e^- efficiency of electroautotrophic CO_2 fixation $\eta_{electro}$ = 99 ± 4% and 95 ± 10% in two independent tests (Entry *1* and *2* in *SI Appendix*, Table S1, respectively). After the three-day electroautotrophy, the visual inspection did not observe any biofilms on the Co–P cathode's surface, nor did images of scanning electron microscopy. There was 30 ± 14 μg of protein from *S. ovata*, a proxy of biomass hence bacterial cell numbers (41), on the electrode, in comparison to the 3,851 ± 147 μg of protein in total from the planktonic cells in the 100-mL reactor. Image analysis of the scanning electron microscopy estimated that a small percentage of the electrode surface, on the order of 0.03 cell μm^{-2}, included attached bacterial cells (*SI Appendix*, Fig. S5). We estimated that the bacterial cells with direct materials contact, necessary but not sufficiently indicative of a direct electron transfer (42), constituted no more than 1% of the predominantly planktonic bacterial cell cultures. Thus, our observations support a near-unity of e^- efficiency for H_2-mediated materials–biology hybrids of CO_2 fixation.

Surprisingly, the e^- efficiency is lower for the microbes grown under chemoautotrophic conditions, even though both electroautotrophic and chemoautotrophic conditions utilize H_2 as the direct reductant for the CO_2-fixing through the Wood–Ljungdahl pathway (36). The headspace of chemoautotrophic *S. ovata* culture was intermittently dosed with mixed gas (H_2:CO_2, 80:20, *v:v*) every 12 h including 2 mmole H_2 substrate (i.e., e^- supply rate of 8 mmole d^{-1}) whose amount was higher than the ones in bioelectrochemical experiments (4.80 ± 0.37 mmole e^- d^{-1}). However, based on temporal trajectory of acetate accumulation, the acetate production rate in chemoautotrophic *S. ovata* culture is 0.48 ± 0.02 mmole d^{-1} (Fig. 1*E* and entry *3* in *SI Appendix*, Table S1), which was lower than 0.67 ± 0.08 mmole d^{-1} in electroautotrophic cultures (Entry *1* in *SI Appendix*, Table S1). Quantifying H_2 consumption in the headspace via gas chromatography established the mass balance of reducing equivalents and led to the averaged apparent e^- efficiency $\eta_{app,chemo}$ of 81 ± 4% (Fig. 1*E*). The corrected e^- efficiency η_{chemo} of 71 ± 4% after subtracting the contribution of extracellular carried-over nutrients (see above) is significantly lower than the $\eta_{electro}$ of 99 ± 4% in the bioelectrochemical case (Entry *1* and *3* in *SI Appendix*, Table S1). Meanwhile, a lower protein yield, a good surrogate of biomass accumulation (16, 43), was observed for chemoautotrophic *S. ovata* (14.9 ± 1.0 μg protein mL^{-1}) than the electroautotrophic ones (20.9 ± 2.1 μg protein mL^{-1}) (*SI Appendix*, Table S1). A small amount of ethanol, ~0.1 mM and ~0.5 mM at 72 h and 120 h, respectively, was observed as another electron sink in chemoautotrophic cultures but not electroautotrophic ones (*SI Appendix*, Fig. S6). Overall, our results suggest that the electroautotrophic *S. ovata* is more efficient in utilizing reducing equivalent H_2 for the acetate production and biomass accumulations.

Additional experiments, originally meant as controls to study the impacts of H_2 delivery conditions, allude to different metabolic conditions between chemoautotrophy and H_2-mediated electroautotrophy. Instead of intermittently dosing *S. ovata* with 80% H_2 at 1 bar pressure that strongly favors CO_2 fixation thermodynamically (44), we aimed to mimic the mass transport and delivery amount of H_2 in electroautotrophy and conducted chemoautotrophic experiments in the same bioelectrochemical setup, with a continuous gas flow of 1% H_2 (H_2:CO_2:N_2, 1:20:79, *v:v:v*) whose H_2 mass transport and delivery amount resemble if not replicate the ones in electroautotrophic conditions (Entry *5* and *6*). Unexpectedly, minimal bacterial CO_2 fixation hence biomass accumulation was observed after multiple attempts (*SI Appendix*, Fig. S7, Entry *5* and *6* in *SI Appendix*, Table S1), different from the chemoautotrophic growth under 80% H_2 (Entry *3* and *4* in *SI Appendix*, Table S1). Multiple attempts of chemoautotrophic culturing under 1% H_2 in the batch mode, which observed the active bacteria growth under 80% H_2, also failed to yield detectable bacterial CO_2 fixation (Entry *7* in *SI Appendix*, Table S1). These observations suggest that the low H_2 partial pressure (1% H_2) disfavoring CO_2 fixation thermodynamically (44) has a significant metabolic impedance of chemoautotrophy, despite the fact that robust microbial CO_2 fixation with high e^- efficiency was observed in electroautotrophy. Our observations lead us to hypothesize that metabolic stimulation and modulation of *S. ovata* are present in the seemingly simple H_2-mediated electrochemical system, warranting detailed comparative, integrated metabolomic, and proteomic studies for a deeper fundamental understanding of the hybrid system.

Observed Metabolomic Shift in Planktonic *S. ovata* Cells Under Electroautotrophic Conditions. There are significant metabolic profile differences between the electroautotrophic and chemoautotrophic planktonic *S. ovata*. To understand the difference, we extracted and measured intracellular metabolites with triplicates (*n* = 3) from the electroautotrophic and chemoautotrophic cultures. Since chemoautotrophic *S. ovata* under 1% H_2 in the bioelectrochemical setup were not active in acetate production, only *S. ovata* active of CO_2 fixation under electroautotrophic and chemoautotrophic conditions with 80% H_2 were collected for subsequent metabolomic and proteomic analyses (Entry *1* and *4* in *SI Appendix*, Table S1, respectively). Out of more than 400 intracellular metabolites involving the majority of metabolic pathways that we searched for, a total of 118 metabolites were measured in both electroautotrophic and chemoautotrophic cultures and 11 metabolites were exclusively detected in electroautotrophic one (Dataset S1). The visualization of the principal component analysis (PCA) with the first two components (Fig. 2*A*), accounting for a combined 77.7% of variance, shows that replicate cultures grown under the same conditions were

grouped together and distant from cultures grown under different conditions, indicating the significant metabolomic difference between electroautotrophic and chemoautotrophic cultures.

Our metabolomic study suggests increased redox cofactor pools in the materials–biology hybrids for CO_2 fixation. The redox cofactors including nicotinamide adenine dinucleotide in both oxidized (NAD^+) and reduced (NADH) forms, and oxidized nicotinamide adenine dinucleotide phosphate ($NADP^+$) all display higher abundance in *S. ovata* cells grown bioelectrochemically, while the concentration ratio between NADH and NAD^+ is 1.5-fold higher in electroautotrophic cells than chemoautotrophic ones (Fig. 2*B*). Such an increase of redox cofactor pool and a more reduced, electron-rich intracellular status may promote a faster turnover of redox-based metabolic activities (45) and a larger driving force for CO_2 reduction (46).

We also analyzed nucleotides as energy cofactors and found out that abundances of adenosine diphosphate (ADP) and adenosine monophosphate (AMP) are threefold higher in electroautotrophic cells than chemoautotrophic cells. Meanwhile, ATP, guanosine diphosphate (GDP), and guanosine monophosphate (GMP) were exclusively detected in electroautotrophic cells (Fig. 2*B*) possibly owing to their lower abundances in chemoautotrophic conditions, molecule instability, and the extended static period required for LC–MS-based metabolomic analysis. Luminescence-based ADP/ATP ratio analysis was conducted and ADP/ATP ratios in electroautotrophic and chemoautotrophic cells are 7.7 ± 0.3 and 9.3 ± 0.5, respectively. The generally high value of ADP/ATP ratio, a lower state of adenylate energy charge, is consistent to the values observed in acetogenic *Acetobacterium woodii* in chemoautotrophy (47), indicative of scarce ATP generation and the thermodynamic limitation in the generally slow-growing acetogens. Yet, the increased pool of nucleotide cofactors and lower ADP/ATP ratio observed in electroautotrophic cells than the chemoautotrophic ones imply a more active cellular metabolism under electricity supply (48).

Moreover, the increased cofactors abundance in H_2-mediated electroautotrophic *S. ovata* is consistent with the abundance changes of key intermediates in the Wood–Ljungdahl pathway (36). Both electroautotrophic and chemoautotrophic samples exhibit detectable amounts of methenyl-tetrahydrofolate (CH-THF) and methyl-tetrahydrofolate (CH_3-THF), hence affording the expression of Wood–Ljungdahl pathway (Fig. 2 *B* and *C*). Yet, acetyl coenzyme A (acetyl-CoA), the key intermediate before the generation of ATP and acetic acid via substrate-level phosphorylation, was only detectable in chemoautotrophic cells. The undesired accumulation of acetyl-CoA in chemoautotrophic cells hints that bacterial cells in the materials–biology hybrid are more efficient in converting acetyl-CoA to acetate for ATP production, a limiting factor of Wood–Ljungdahl pathway (36), consistent with the lower ADP/ATP ratio in electroautotrophy than chemoautotrophy

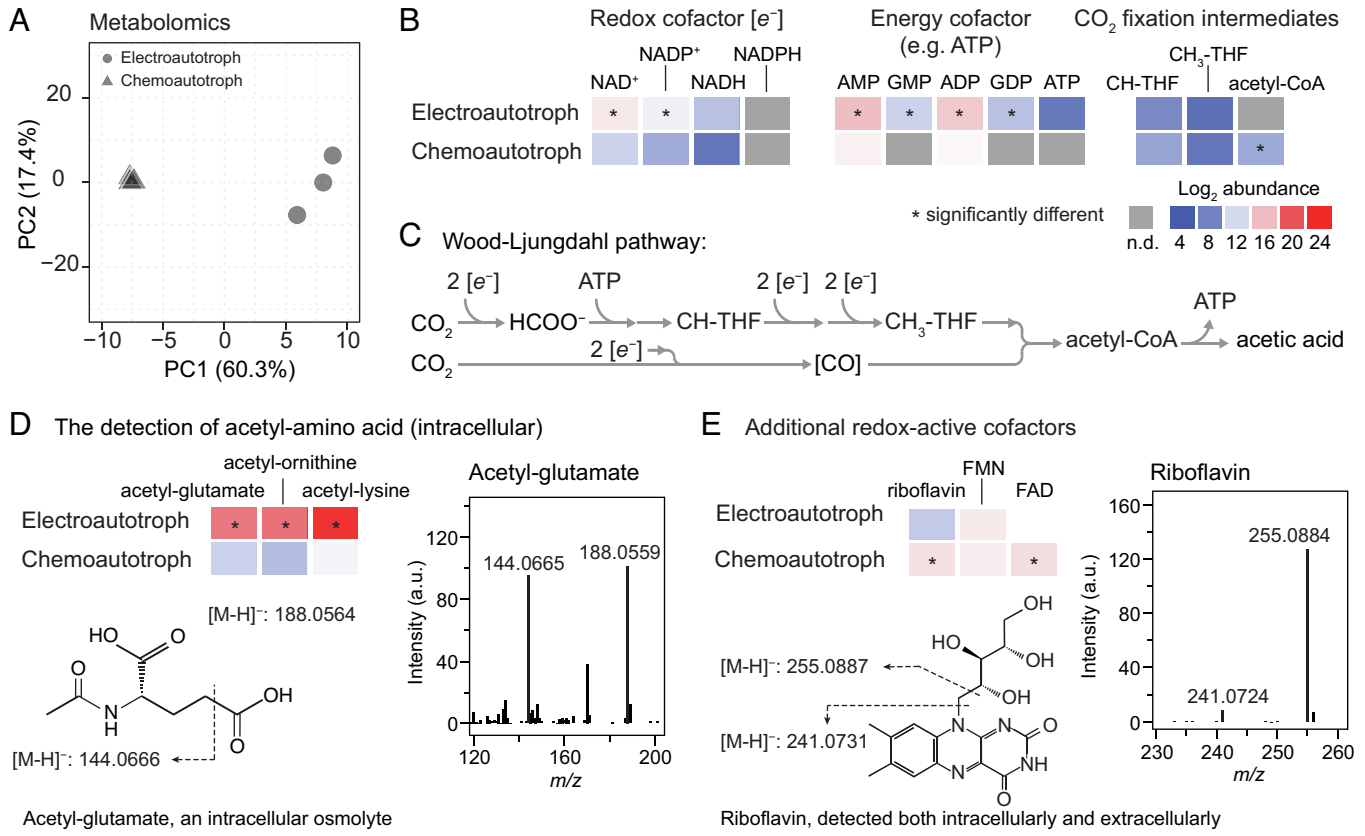

Fig. 2. Metabolomic shift in planktonic *S. ovata* cells induced by electroautotrophy. (*A*) The principal component analysis (PCA) of intracellular metabolomes extracted from *S. ovata* cells grown under both electroautotrophic (gray circle) and chemoautotrophic (gray triangle) conditions. Each symbol represents one of three biological replicates. (*B* and *C*) Heatmaps visualizing abundance changes of metabolites involved in the Wood–Ljungdahl pathway including redox cofactors, energy cofactors, and CO_2 fixation intermediates. (*D* and *E*) Abundances and tandem mass spectra of intracellular acetyl-glutamate (*D*) and intracellular riboflavin (*E*). Riboflavin was also detected extracellularly (Dataset S1). Panels (*B*, *D*, and *E*) share the same color legend which is shown in panel (*B*). Numerical results for metabolite abundance are shown in Dataset S1. *, significant difference between conditions (fold change ≥ 2 and $P < 0.05$); n.d., not detected; NAD^+ and NADH, Nicotinamide adenine dinucleotide; $NADP^+$ and NADPH, nicotinamide adenine dinucleotide phosphate; AMP, adenosine monophosphate; GMP, guanosine monophosphate; ADP, adenosine diphosphate; GDP, guanosine diphosphate; ATP, adenosine triphosphate (ATP); CH-THF, methenyl-tetrahydrofolate; CH_3-THF, methyl-tetrahydrofolate; acetyl-CoA, acetyl coenzyme A; FMN, flavin mononucleotide; FAD, flavin adenine dinucleotide.

(7.7 ± 0.3 vs. 9.3 ± 0.5) and a faster kinetic of ATP production. Those results corroborate a CO_2-fixing mechanism in electroautotrophy not only more active but also more energy efficient in the context of ATP generation.

There are two more noteworthy metabolomic differences between electroautotrophic and chemoautotrophic cells. First, one of the largest abundance changes of intracellular metabolites is the 150-fold to 500-fold increase of N-acetyl-amino acids, such as acetyl-glutamate, acetyl-ornithine, and acetyl-lysine, in the electroautotrophic cells (Fig. 2*D*). The magnitude of such abundance change, in conjunction of their possible implication towards the osmotic protection (49), offers some intriguing clues toward a hypothesized shift of membrane electrochemical potential ($\Delta\mu_{proton}$) in the materials–biology hybrid (see below). Second, we attempted extracting the extracellular metabolites in both scenarios and searching for additional extracellular redox mediators. Intracellularly, RAMs including riboflavin (Fig. 2*E*), flavin adenine dinucleotide (FAD), and flavin mononucleotide (FMN) (*SI Appendix*, Fig. S8) were detected under both electroautotrophic and chemoautotrophic conditions. Yet, only riboflavin was also detected extracellularly under both conditions, albeit at a much diluted concentration on the order of nmol/L. Comparison of riboflavin abundance suggests that there is no statistically significant difference for extracellular riboflavin between electroautotrophy and chemoautotrophy (Dataset S1), while chemoautotrophy witnessed a higher abundance of intracellular riboflavin (Fig. 2*E*). The extracellular concentration of riboflavin is too low to contribute significantly if anything to the delivery of reducing equivalent and CO_2 fixation but may serve as a signal molecule toward an altered microbial metabolism in the H_2-mediated materials–biology hybrids.

Materials-Induced Differential Gene Expression during Electroautotrophic Conditions. A total of 1,993 proteins of *S. ovata* were detected in chemoautotrophic and electroautotrophic cultures (detailed annotations and abundances are available in Dataset S2), among the annotated *S. ovata* DSM2662 genome encoding 5,103 proteins (Uniprot Proteome ID: UP000015521) (50). In addition, 1,697 proteins were stably expressed (fold change < 1.5) under both conditions (Fig. 3*A*). Among the five hydrogenases that were annotated in the genome of *S. ovata* (51), one [NiFe] hydrogenase and two [Fe] hydrogenases were detected with similar level of expression. Such results support H_2 as the primary energy source for microbial CO_2 fixation under both chemoautotrophic and H_2-mediated electroautotrophic conditions and that the rate of H_2 delivery should not contribute significantly to the observed difference in e^- efficiency. All the enzymes involved in the Wood–Ljungdahl pathway including formate dehydrogenase (FdhA), formyl-THF synthase (Fhs), methenyl-THF cyclohydrolase (FchA), methylene-THF dehydrogenase (FolD), methylene-THF reductase (MetFV), CO dehydrogenase/Acetyl-CoA synthase (AcsABCDEFV and CooC), and acetate kinase (AckA) were all

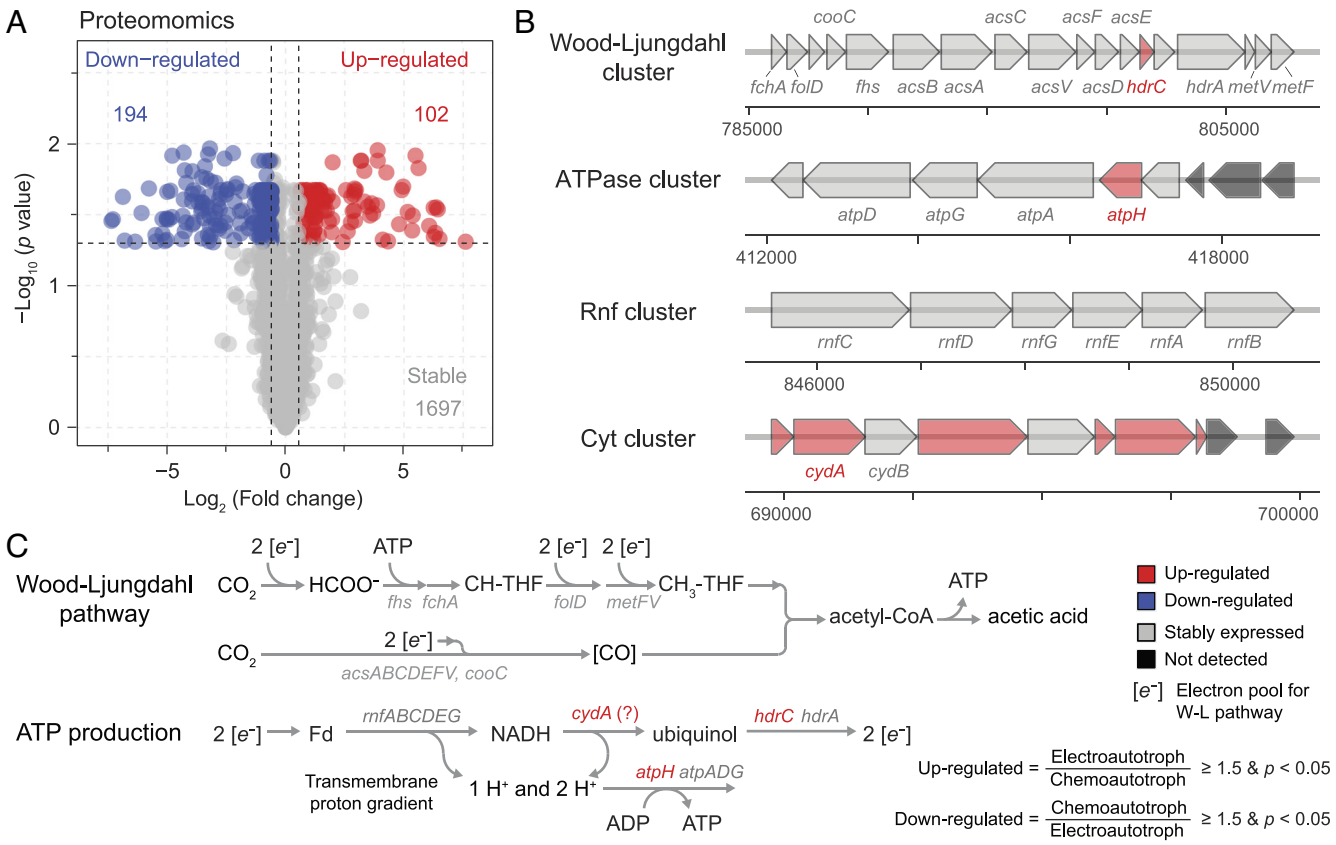

Fig. 3. Electrochemical system–induced differential gene expression in *S. ovata* cells. (*A*) Volcano plot demonstrating detected proteins in electroautotrophic and chemoautotrophic cells. The differentially expressed proteins between electroautotroph/chemoautotroph and chemoautotroph/electroautotroph were determined by fold change ≥ 1.5 and $P < 0.05$. The number in color represents the number of proteins determined in the associated category. (*B*) Expression of gene clusters of interest. The Wood–Ljungdahl cluster includes genes for methenyl-THF cyclohydrolase (*fchA*), methylene-THF dehydrogenase (*fold*), CO dehydrogenase/acetyl-CoA synthase (*cooC* and *acsABCDEFV*), formyl-THF synthetase (*fhs*), heterodisulfide reductase (*hdrAC*), and methylene-THF reductase (*metFV*) involved in the Wood–Ljungdahl pathway. The ATPase cluster contains genes for ATP synthase (*atpADGH*). The Rnf cluster includes genes encoding ferredoxin:NAD^+ oxidoreductase (*rnfABCDEG*). The Cyt cluster contains genes for cytochrome *bd* (*cydAB*). (*C*) The involvement of the expressed proteins in the Wood–Ljungdahl pathway and the speculative ATP production pathway. Numerical results for protein abundance are shown in Dataset S2. Ferredoxin (Fd).

stably expressed in both electroautotrophic and chemoautotrophic cells (Fig. 3 *B* and *C*). The lack of statistically significant changes in abundance indicates that microbial capability of CO_2 fixation into acetic acid remained unperturbed in the materials–biology hybrid. Such result also suggests that other factors connected to but not within the Wood–Ljungdahl pathway, such as ATP generation as one key limiting factor for acetogenic organisms (see above) (52), are potentially responsible for the observed difference in e^- efficiency (Fig. 1 *D* and *E*).

We also observed significant differences (fold change ≥ 1.5 and $P < 0.05$) of gene expressions in some key proteins that hints a favored membrane-based proton translocation and ATP generation in *S. ovata* grown electroautotrophically. Differential gene expression was observed that 102 proteins were up-regulated in *S. ovata* cells grown with electrochemical system while 194 proteins were up-regulated in cells grown under H_2-containing headspace (Fig. 3*A*). Notably, the subunit of ATP synthase (AtpH), the enzyme responsible for ATP generation based on proton translocation (53), is up-regulated in the materials–biology hybrid (Fig. 3*B*). This corroborates an enhanced ATP production under the bioelectrochemical condition as observed in metabolomic analysis. Meanwhile, ferredoxin:NAD^+ oxidoreductase (Rnf) and heterodisulfide reductase subunit C (HdrC), the two enzymes that are reported to sequentially translocate H^+ and generate transmembrane proton gradient by a series of membrane-bound electron transfer (54–56), are either stably expressed for Rnf or up-regulated for HdrC. Such information suggest that the establishment of transmembrane H^+ gradient is favored in the electroautotrophic condition. Such an argument is corroborated by the observed upregulation of cytochrome *bd* ubiquinol oxidase (Cyt *bd*) subunit A (Cyd A) and several proteins neighboring the same gene cluster (Fig. 3*B*), which are the putative components of the electron transport chain that connects HdrC via ubiquinol pool (Fig. 3*C*) (56). Meanwhile, the Na^+/H^+ antiporter (Nha) involved in maintaining cytosol pH homeostasis (57) was found significantly upregulated under electroautotrophic conditions. This observation suggests a shift and possible regulation of $\Delta\mu_{proton}$ in electroautotrophic *S. ovata* cells as discussed in-depth below.

Integrated Omic-Analysis Unraveled Metabolic Rewiring. Our experimental observations collectively support a more active and efficient metabolism in the materials–biology hybrid, for the generation of energy carriers and the reduction of CO_2 into acetic acid. We demonstrated a H_2-mediated electroautotrophy, based on the absence of noticeable biofilm formation on Co–P alloy cathode (*SI Appendix*, Fig. S5), the estimated percentage of more than 99% for planktonic cells, and the inability of detecting other known redox mediators at appreciable concentrations (>nM). We observed an accelerated production of acetic acid and increased values of e^- efficiency (Fig. 1 *D* and *E* and *SI Appendix*, Table S1), even though the hybrid system consumed similar amounts of reducing equivalent namely H_2 as the chemoautotrophic ones do under the similar levels of hydrogenase expression in both conditions. Additional experiments under different methods of H_2 delivery suggest that mass transport of H_2 does not contribute to such observed differences of e^- efficiency. Instead, it is the significant difference in thermodynamic Gibbs free energies of CO_2 reduction (ΔG) under different H_2 partial pressures that leads to drastic observed difference of chemoautotrophic CO_2-fixing rates between 1% and 80% H_2 partial pressure. ΔG is calculated to be –16.7 and –27.8 kJ/mol per one equivalent of H_2 for 1% and 80% H_2 partial pressures at 1 bar, respectively, under otherwise the same physiological conditions (*SI Appendix*, Fig. S9). It is remarkable that the more efficient electroautotrophy (Entry *1* and *2* in *SI Appendix*, Table S1) occurs at a much lower H_2 partial pressure, i.e., against a less favored ΔG, than the compared chemoautotrophic ones with 80% H_2 at 1 bar in the headspace (Entry *3* and *4* in *SI Appendix*, Table S1).

Meanwhile, the abundance of redox-active and more importantly non-redox-based energy cofactors, quantitatively assayed via measuring the NADH/NAD^+ and ADP/ATP ratios, indicated that intracellular conditions in the hybrid system were more reduced and energy-rich (Fig. 2*B*), while the metabolic activities and protein expressions in the Wood–Ljungdahl pathway remained largely unperturbed (Figs. 2*B* and 3*B*). Such an enhanced metabolic energy supply was consistent with the up-regulated expression of ATP synthase and other proteins related to the generation of transmembrane proton gradient (Fig. 3 *B* and *C*). In the Wood–Ljungdahl pathway (36), acetogenic organisms are quite ATP-limited under chemoautotrophic conditions due to the net zero ATP synthesis by substate-level phosphorylation. The organisms are predicted to yield at most 0.5 to 1.5 ATP through the transmembrane H^+ gradient for each acetic acid molecule after an 8-electron reduction of CO_2 (58, 59). Hence, our observations suggest that the efficiency of ATP generation in *S. ovata* was increased in the materials–biology hybrid.

We hypothesize that the up-regulated expression of Hdr and cytochromes contribute to an increased H^+ translocation hence microbial generation of ATP in electroautotrophic conditions (Fig. 4). *S. ovata* is reported to generate transmembrane proton gradient hence ATP through a confurcation mechanism (56), in which ferredoxin generated by electron-bifurcating hydrogenase (Bif) first transforms to NADH via proton-pumping Rnf and subsequently to NAD^+ via a H^+-pumping electron transport chain including ubiquinol, Hdr, and speculatively cytochromes (Cyt) (Fig. 4). Our observed upregulation of Hdr and cytochromes will potentially increase the extent of the second H^+-pumping step by the confurcation mechanism. Such metabolic shift in the materials-biology hybrid can alleviate the limited ATP yield with faster microbial CO_2 fixation and a higher e^- efficiency.

A relevant side evidence supporting the proposed increase of proton translocation resides in the observed significant upregulation of Na^+/H^+ antiporter (Nha) expression and the increased accumulation of N-acetyl-glutamate in the H_2-mediated materials-biology hybrids (Fig. 4). While there is a sufficient thermodynamic driving force of CO_2 fixation at 80% H_2, at low H_2 partial pressure as the case of electroautotrophy, it is critical to maintain a homeostasis of suitable membrane proton electrochemical potential ($\Delta\mu_{proton}$), typically –140 to –200 mV as commonly reported (57), in order to satisfy two contradicting factors for sustained CO_2 fixation (*SI Appendix*, Fig. S10, more detailed discussion in *SI Appendix*, *Supplementary Note* 2). First, a negative enough $\Delta\mu_{proton}$ must be maintained in order to have sufficient energy to drive ATP formation owing to the structural H^+/ATP stoichiometry of ATP synthase (60); second, $\Delta\mu_{proton}$ cannot be too negative in order to thermodynamically enable H^+-pumping in aforementioned coupling sites driven by exergonic redox reactions (57). Therefore, ideally a suitable $\Delta\mu_{proton}$ level tailored to the specific H_2 partial pressure must be maintained to enable CO_2 fixation in acetogens, and a less negative $\Delta\mu_{proton}$ better suits a lower H_2 partial pressure owing to change of ΔG values for CO_2 fixation. As Na^+/H^+ antiporter (Nha) is known to modulate pH homeostasis by exchanging extracellular H^+ with intracellular Na^+ hence increasing the value of $\Delta\mu_{proton}$ (*SI Appendix*, *Supplementary Note* 2 and Fig. S10), our observed significant upregulation of Nha during electroautotrophy is consistent with the expected shift of $\Delta\mu_{proton}$ for sustained CO_2 fixation under low H_2 partial pressure. Similarly, the accumulation of acetyl-glutamate, a common osmolyte (49), could

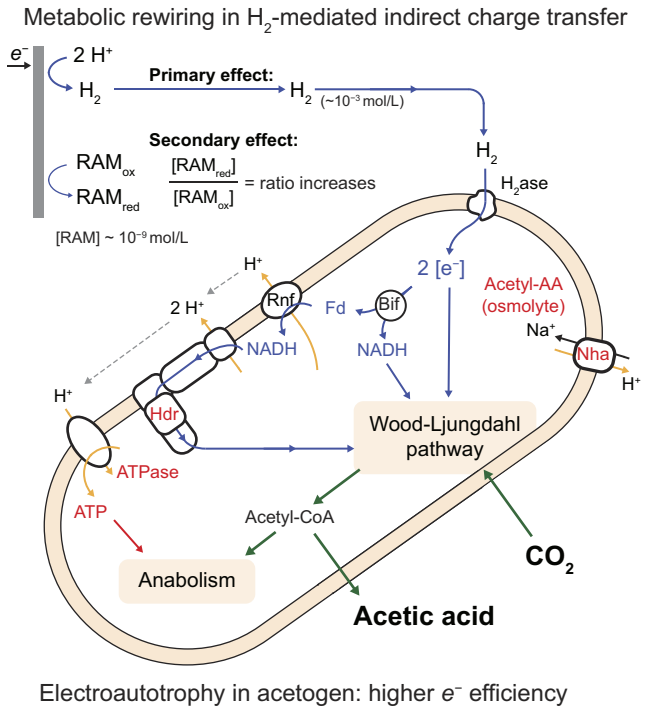

Fig. 4. Proposed metabolic rewiring in electroautotrophic *S. ovata*. The enzymes in black are stably expressed under both electroautotrophic and chemoautotrophic conditions, while the enzymes in red were up-regulated under electroautotrophic conditions. The metabolites in red were more abundant in electroautotrophic cultures. Blue arrows represent electron flow, and green arrows represent carbon flow in *S. ovata* metabolism. The proton translocation and ATP synthesis are highlighted by yellow arrows. RAM_{ox} and RAM_{red} are the oxidized and reduced redox-active metabolites, respectively; H_2ase, hydrogenase; Bif, electron-bifurcating hydrogenase; Nha, Na^+/H^+ antiporter; Acetyl-AA, acetyl-amino acids.

be explained as a response toward the increased osmotic pressure due to the extensive loss of intracellular Na^+. The electroautotrophic condition is hypothesized to rewire the metabolism by modulating $\Delta\mu_{proton}$ and achieve a balance between proton-pumping at coupling sites and ATP synthesis, which is not present under chemoautotrophic conditions under similarly low H_2 partial pressure.

Metabolic Rewiring Hypothetically Based on Extracellular Redox-Active Metabolites (RAMs). We hypothesize that it is the trace amount of extracellular RAMs such as riboflavin detected in our experiments that putatively signal the metabolic rewiring. The stable expression level of hydrogenase, as well as the slow if any chemoautotrophic CO_2 fixation under similarly low H_2 pressures, preclude H_2 as the signaling pathway in electroautotrophy. Therefore, other signaling pathways, probably redox-based, must be present in addition to the H_2-mediated materials-biology hybrids. We detected intracellular FAD, FMN, and riboflavin in all tested conditions (Fig. 2*E* and *SI Appendix*, Fig. S8). Small amount of extracellular riboflavin was also detected at most on the order of nM (Dataset S1), which is too low to contribute significant delivery of reducing equivalents for CO_2 fixation. Yet, such extracellular riboflavin exhibits reversible redox peaks in cyclic voltammograms with the half-wave potential ($E_{1/2}$) of –0.209 V vs. SHE (*SI Appendix*, Fig. S11), in accordance with the reported value of –0.210 V vs. SHE (61). Because riboflavin is electrochemically redox active (62), riboflavin will be almost exclusively under its reduced form under the electroautotrophic conditions of electrochemical H_2 generation (–0.77 to –0.96 V vs. SHE). Such a predominantly reduced population of extracellular riboflavin should differ appreciably from the one under chemoautotrophic condition when direct reduction of riboflavin by H_2 is kinetically slow in the absence of catalyst (63).

Soluble redox-active electron shuttles, commonly derivatives of flavins, quinones, phenazines, and cytochromes, are known to mediate long-distance electron transfer at a redox potential close to HER (64, 65) and trigger metabolic rewiring in microorganisms (66, 67). Therefore, our observed presence and electroactivity of extracellular riboflavin lead us to propose that the extracellular riboflavin, along with other possible extracellular RAMs, should serve as redox-sensing signal molecules. Because extracellular riboflavin's abundance does not change significantly between electroautotrophic and chemoautotrophic samples, we deem the redox states of extracellular riboflavin, instead of the absolute concentration, that contributes to the observed metabolic rewiring. The proposed ratiometric signaling, based on the concentration ratio between reduced and oxidized riboflavin, is consistent with the regulation of microbial activities by altering the redox status of the extracellular RAMs (Fig. 4), which has been exemplified in the case of pyocyanin for bacterium *Pseudomonas aeruginosa* (68). This ratiometric figure-of-merit is also in line with the fact in bioenergetics that it is the ratiometric values including [NAD(P)H]/[NAD(P)$^+$] and adenylate energy charge that fundamentally govern microbial metabolism (69). We hypothesize that this previously underappreciated redox signaling in *S. ovata* system triggers the observed metabolic rewiring including a tailored $\Delta\mu_{proton}$ level, up-regulated Hdr and Cyt for proton translocation, more efficient ATP generation, and a more reduced intracellular redox state for H_2-mediated microbial CO_2 fixation (Fig. 4).

Our reported metabolic rewiring shares some similarities yet differs from previous literature precedencies related to electrofermentation (12, 70). Acetogens under heterotrophic fermentation, such as *Clostridium acetobutylicum* (71), are known to shift the fermentation product distribution toward more reduced chemicals under the presence of exogenous mediators such as viologens, commonly under a reductive electrochemical driving force (72). It is similar that both our case and the ones of electrofermentation (72) witness a more reduced cellular redox state. Yet, the reported autotrophic metabolism differs greatly from the heterotrophic fermentation because the limiting factor here is the limited ATP generation owing to the small thermodynamic energy gain of acetogenesis and the zero net ATP yield from substrate-level phosphorylation in the Wood–Ljungdahl pathway (36), while ATP generation in heterotrophic fermentation is not a major concern. Hence, the major impacts from the varied redox states of extracellular riboflavin reported here reside on the proton translocation and ATP synthesis that leads to the observation of a smaller ADP/ATP ratio during electroautotrophy, which is significantly different from the previous reports in electro-fermentation (70, 72). Indeed, the fact that only chemoautotrophic cultures yield ethanol (*SI Appendix*, Fig. S6), the more reduced product than acetate, corroborates the aforementioned difference between our case and the ones of electro-fermentation, when more reduced products were promoted under additional electrochemically reductive energy input (70, 72).

Discussion

In this work, we showcase the previously undetected metabolic rewiring in *S. ovata* from a H_2-mediated materials-biology hybrid. Such results illustrate the metabolic versatility and complexity of *S. ovata*, thanks to its high e^- efficiency of CO_2 fixation (73),

robustness toward extragenic interferences (74), and the plentiful redox-based coupling sites involving ubiquinol and cytochromes (55). Future studies about the detailed signaling pathway between the microbes and the water-splitting electrodes, currently proposed via the mediation of extracellular riboflavin, will be welcomed and should yield useful insights about proton translocation and ATP generation that are critical in the CO_2-fixing Wood–Ljungdahl pathway. Such insights will be beneficial for the design of hybrid systems for sustainable CO_2 fixation with *S. ovata* as the biotic component.

Moreover, our unexpected observation of the fortuitous metabolic rewiring highlights the necessity of thorough examination about the interactions in materials–biology hybrids. We posit that the observed metabolic rewiring may exist in a wide range of seemingly simple H_2-mediated hybrid systems with potential benefits that so far have been under-appreciated and under-utilized. In addition to the extensive research efforts being devoted toward materials design and synthetic biology for the efficient production of targeted chemicals in the hybrids (1, 2, 4), we advocate the deployment of multiomic studies for a comprehensive understanding of microbial metabolism in search of unexpected synergies. Such research efforts will enable us to maximize the efficiency and throughput of CO_2 fixation using the materials-biology hybrids for a sustainable future.

Materials and Methods

Materials and Chemicals. The chemicals and materials were purchased from Sigma-Aldrich, unless otherwise specified. The carbon cloth was purchased from Fuel Cell Earth, and the stainless-steel mesh was purchased from Alfa Aesar. The ^{1}H NMR standard sodium 3-(trimethylsilyl) propionate 2,2,3,3-D4 (TSP-D4) and deuterium oxide (purity > 99.9%) were obtained from Cambridge Isotope Laboratories, Inc. Methanol, acetonitrile, ammonium acetate, ammonium hydroxide, and acetic acid were purchased from Fisher Scientific.

Electrode Fabrication and Characterization. The cathode and anode were coated with Co–P alloy and cobalt phosphate (CoPi) catalysts, respectively, using electrochemical deposition following established protocols (7, 14, 31). A single-chamber electrochemical setup installed with a working electrode of deposition substrate, a Pt counter electrode, and a Ag/AgCl (3M KCl) (CH Instruments) reference electrode was connected to Gamry Interface 1000 potentiostat (Gamry Instruments). The Co–P alloy cathode was prepared by a 15-min chronoamperometry in an electrolyte consisted of 0.15 M H_3BO_3, 0.1 M NaCl, 0.33 M $NaH_2PO_2{\cdot}H_2O$ (sodium hypophosphite), and 0.2 M $CoCl_2{\cdot}6H_2O$, during which the stainless-steel mesh was poised at –1.5 V vs. reference electrode. The CoPi anode was deposited on the carbon cloth in an electrolyte consisted of 10 mM $Co(NO_3)_2$ and 0.1 M methylphosphonate with a pH adjustment to 8. Chronocoulometry was performed with an applied potential of 0.85 V vs. reference electrode until 500 mC cm^{-2} of charge was transferred.

The morphologies and element compositions of electrocatalysts (*SI Appendix*, Fig. S2) were characterized by JEOL JSM-6700F field emission scanning electron microscope (JOEL) equipped with Ametek energy-dispersive X-ray spectroscopy (EDS) device (EDAX-AMETEK) or ZEISS Supra 40VP field emission scanning electron microscope (ZEISS), after Au sputtering with Hummer 6.2 sputter coater (Anatech). A pretreatment followed an established protocol (33) was applied for the electron microscopy characterization of Co–P cathode with potentially adhered cells. The cathode was fixed in 2.5% glutaraldehyde overnight and sequentially immersed in ethanol (25%, 50%, 75%, 90%, 100%, 10 min each) and then transferred into hexamethyldisilazane (HMDS) for 1 h. The cathode was left to air dry overnight prior to characterization.

Chemoautotrophic Culturing of *S. ovata*. The *S. ovata* were routinely maintained at 30 °C in 160 mL serum bottles containing 100 mL of mineral salts medium (75, 76) (*SI Appendix*, *Supplementary Note* 1) closed with butyl rubber stoppers (Chemglass Life Sciences LLC) held in place with aluminum crimps. The headspace was filled with 1-bar H_2:CO_2 (80:20, *v*:*v*) with sufficient agitation. For the growth comparison under different conditions, the inoculum of H_2-grown *S. ovata* cells was transferred in biological triplicates.

The chemoautotrophic cultures were grown at 30 °C in the 160-mL serum bottle containing 50 mL mineral salts medium (*SI Appendix*, *Supplementary Note* 1), 50 mL inoculum, and 60 mL headspace, which were maintained under similar if not the same experimental conditions as the electroautotrophic cultures except for the electron donor (see below). H_2 was intermittently supplied to the chemoautotrophic cultures by replacing the headspace (60 mL) with H_2:CO_2 (80:20, *v*:*v*) every 12 h at 1 bar with sufficient agitation. Under such conditions, *S. ovata* utilized H_2 as the sole electron donor and CO_2 and $NaHCO_3$ as the carbon sources. All cultures were grown under strictly anoxic conditions in the presence of reducing reagents of 0.2 mM Na_2S and 0.2 mM cysteine. At least two independent batch experiments, each with three replicates, were performed for the sake of reproducibility (Entry *3* and *4* in *SI Appendix*, Table S1). A negative control was performed on the same medium for *S. ovata* growth in the absence of electricity or H_2, and the headspace was replaced by N_2:CO_2 (80:20, *v*:*v*) every 12 h at 1 bar (*SI Appendix*, Fig. S3). To mimic the mass transport in electroautotrophic cultures (see below), chemoautotrophic growth of *S. ovata* was also tested in the same bioelectrochemical setup (see below) yet in the absence of electricity (Entry *5* and *6* *SI Appendix*, Table S1). Instead, a continuous gas flow of H_2:CO_2:N_2 (1:20:79, *v*:*v*:*v*) was bubbled to the setup from the gas tube submerged around 2 cm below the liquid surface, mimicking if not replicating the mass transport and the delivery of H_2 in electroautotrophy, under similar electron supply rate and agitation rate (i.e., 150 rpm) as the electroautotrophic cultures except for the electron donor. Two different gas flow rates of 4 mL min^{-1} and 6 mL min^{-1}, controlled by the mass flow controller (Omega Engineering), were tested with almost the same results (Entry *5* and *6* in *SI Appendix*, Table S1). Aliquot samples were taken from the cathodic chamber periodically for further analysis.

Electroautotrophic Materials–Biology Hybrids of *S. ovata*. The electroautotrophic cultures were established with triplicates following previously reported procedure with slight modifications (31). Customized three-electrode, two-chamber (150 mL each) electrochemical cells (H cells), separated by Nafion 117 membrane (Chemours), were applied for *S. ovata* incubation to allow the proton exchange (*SI Appendix*, Fig. S1). The gas-tight cathodic chamber had been flushed with N_2:CO_2 (80:20, *v*:*v*) to maintain the anoxic environment, followed by the transfer of the mineral salts medium (50 mL) and *S. ovata* inoculum (50 mL) under strict anoxic conditions. The cathode chamber includes Co–P cathode (2 × 2 cm) and leak-free Ag/AgCl reference electrode (+0.209 V vs. standard hydrogen potential, SHE, Innovative Instruments, Inc.) under a constant gas supply of N_2:CO_2 (80:20, *v*:*v*) at the rate of 6 mL min^{-1} controlled by the mass flow controller. In order to maintain similar if not the same gas transport as the case of chemoautotrophic growth (see above), the gas supply is purged over the headspace of cathodic chamber. The anodic chamber includes CoPi anode and the headspace was continuously flushed with N_2:CO_2 (80:20, *v*:*v*). Both chambers were stirred at the constant rate of 150 rpm and placed in a water bath maintained at 30 °C during the three-day experiment. Aliquot samples were taken from the cathodic chamber periodically for further analysis.

The electrochemical settings of electroautotrophic cultures were achieved with a Gamry Interface 1000E potentiostat interfaced with a Gamry 8-channel ECMB multiplexer. The electrochemical potentials (*E*) have been *iR* compensated with the solution series resistance determined daily by electrochemical impedance spectroscopy and are all referenced to SHE using the following Eq. **1**:

$$E \text{ vs. SHE} = E \text{ vs. Ag/AgCl} + 0.209 \text{ V}. \quad [\mathbf{1}]$$

Cyclic voltammetry (CV) between –0.39 V to –1.39 V vs. SHE at a scan rate of 50 mV s^{-1} was conducted daily to check the system's stability. Multiplexed chronoamperometry, whose *E* values are adjusted daily to maintain a desired level of current intensity, was performed to ensure electroautotrophic systems.

Residual Extracellular Oxidizable Organics Carried Over during Bacterial Inoculation. The chemical oxygen demand (COD) in the extracellular components of the culture after *S. ovata* inoculation was analyzed in order to more accurately quantify the e^- efficiency of CO_2 fixation. The extracellular components were collected by filtering culture through sterile polyethersulfone membrane (0.22 μm, Avantor) to exclude planktonic *S. ovata* cells. Colorimetric COD analysis was performed using TNT82206 kit (Hach) following the manufacturer's protocol,

after establishing a standard curve prepared in the same mineral salts medium to avoid any matrix effects interfering with the quantification. The potential electron storage in the extracellular oxidizable component in carryover was calculated based on Eq. **2**.

$$N_{e,carryover}(mmole) = COD(mmole) \times 4 - N_{acetate}(mmole) \times 8. \quad [2]$$

Here, COD represents the amount of oxygen required to completely oxidize the extracellular components, $N_{acetate}$ the observed generation of extracellular acetate (see below), and $N_{e,carryover}$ presents the amount of reducing equivalents, in the unit of millimoles (mmole) of electrons, that can contribute to bacterial CO_2 fixation. Here, we assume that 1 COD equivalent offers 4 electron equivalents and the formation of one equivalent acetate requires 8 electron equivalents via CO_2 fixation.

Product Quantification and Electron Efficiency Analysis. The liquid products in the sampled aliquots were quantified by the 400 MHz NMR spectrometer (Bruker) equipped with Bruker AV400 Sample Changer. Representative ^{1}H-NMR spectra under chemoautotrophic conditions are provided in *SI Appendix*, Fig. S6. While the electroautotrophic cultures almost exclusively yield acetate, chemoautotrophic cultures yields small amount of ethanol and occasionally formic acid as an ephemeral product. We note the technical difficulties of accurate quantification of low-level ethanol concentrations as our Hungate anaerobic technique demands gas purging despite ethanol's high volatility. The acetate concentration was quantified using the chemical shift of 1.92 ppm in ^{1}H NMR spectroscopy on a liquid sample containing culture suspension and internal standard of TSP-D4 (31), after the establishment of a standard calibration curve. The total amount of acetate accumulation was calculated based on the measured acetate concentration and liquid volume. The H_2 partial pressure in the culture headspace was measured by an 8610C gas chromatography system (SRI Instruments) equipped with Hayesep D and MS 5A packed columns, and a thermal conductivity detector (TCD) (16). The total amount of H_2 in the liquid culture was calculate every 12 h based on measured H_2 partial pressure, by considering both the gaseous and dissolved H_2 with additional inputs of the monitored headspace gas pressure (McMaster-Carr) and the known H_2 solubility with a Henry solubility coefficient of 7.7×10^{-6} mole m^{-3} Pa^{-1} (77). Last, the protein concentrations in *S. ovata* cultures were determined using the Bradford assay following an established protocol (43). Lysed culture suspension was prepared by treating 0.5 mL culture suspension in a boiling water bath and then mixed with Pierce Coomassie reagent (Pierce Coomassie Protein Assay Kit, Thermo Scientific) for a colorimetric analysis of 595-nm absorbance using Cary 60 UV-Vis spectrophotometer (Agilent Technologies), following the manufacturer's protocol after establishing a calibration curve with albumin as the standard sample. To quantify proteins in cells attached to Co–P cathode, the Co–P cathode (2 × 2 cm) was collected after incubation and immediately immersed in 1 mL cell-free mineral salts medium followed by the same extraction procedures. At the same time, the extraction control including the Co–P cathode but without electroautorophic incubation was conducted and returned no protein detection, suggesting that the extraction procedures will not lead to false positive observations in the Bradford assay.

The apparent electron efficiencies (e^- efficiencies) η_{app} under electroautotrophic and chemoautotrophic conditions ($\eta_{app,electro}$ and $\eta_{app,chemo}$, respectively), without considering potential contribution from the extracellular organics carried over from inoculation, were calculated using Eqs. **3** and **4**, respectively.

$$\eta_{app,electro} = \frac{\Delta C_{acetate} \times V_{medium} \times 8}{\int_{t_0}^{t} I dt \times F} \times 100\%, \quad [3]$$

$$\eta_{app,chemo} = \frac{\Delta C_{acetate} \times V_{medium} \times 8}{\Delta N_{H_2} \times 2} \times 100\%. \quad [4]$$

Here, $\Delta C_{acetate}$ represents concentration change of acetate that each requires 8 electrons from CO_2 reduction, V_{medium} the total volume of liquid culture, $\int_{t_0}^{t} I dt$ the total amount of charge transfer during electroautotrophy, F the Faraday constant (96,485 C mole^{-1}), and ΔN_{H_2} the amount of H_2 consumed during chemoautotrophy that each contributes two electrons for CO_2 reduction.

Moreover, because we found that the extracellular organics carried over from bacterial inoculation contribute appreciable amount of reducing equivalents toward bacterial metabolism (see above), it is more appropriate to calculate the corrected e^- efficiencies η by accounting the reducing equivalents in extracellular organics ($N_{e,carryover}$) for both electroautotrophic ($\eta_{electro}$) and chemoautotrophic (η_{chemo}) conditions, respectively:

$$\eta_{electro} = \frac{\Delta C_{acetate} \times V_{medium} \times 8}{\int_{t_0}^{t} I dt \times F + N_{e,carryover}} \times 100\%, \quad [5]$$

$$\eta_{chemo} = \frac{\Delta C_{acetate} \times V_{medium} \times 8}{\Delta N_{H_2} \times 2 + N_{e,carryover}} \times 100\%. \quad [6]$$

Both apparent and corrected e^- efficiencies under each experimental condition were reported in *SI Appendix*, Table S1.

Luminescence-Based ADP/ATP Ratio Analysis. The two-step D-luciferin-based ADP/ATP ratio analysis was performed using MAK15 kit (Sigma-Aldrich) following the manufacturer's protocol. Then, 10 µL bacterial culture under both electroautotrophic and chemoautotrophic conditions was collected immediately after the three-day experiments and instantly mixed with reaction reagent on a 96-well plate with a clear bottom. The luminescence intensities were recorded by microplate reader SpectraMax iD3 (Molecular Devices) and the ADP/ATP ratio was calculated following the manufacture's protocol.

Metabolome Extraction and Sample Preparation. After a three-day experiment, 1-mL bacterial suspension was vacuum-filtered on a nylon membrane (25 mm diameter, 0.2 µm pore size, Millipore). The membrane was immediately transferred to a 6-well plate containing 1 mL of cold extraction solvent for non-folate species (–20 °C, 40:40:20, methanol/acetonitrile/water) to quench metabolism. For intracellular folate species, the extraction solvent was 80:20 acetonitrile/water with 2.5 mM sodium ascorbate and 25 mM ammonium acetate stored at 4 °C for stability. After 20 min of metabolite extraction at the respective cold temperatures, the cell extract was collected, transferred to a microcentrifuge tube, and centrifuged at 17,000 × g for 10 min at 4 °C. The supernatant was transferred to a new centrifuge tube, dried under nitrogen flow, and reconstituted in LC–MS (liquid chromatography-mass spectrometry) grade water before transferring to vials for LC-MS analysis (78). Additionally, to determine extracellular metabolites, the filtrate of bacterial suspension was diluted with LC–MS grade methanol at a 20:80 ratio. After centrifuging at 17,000 × g for 10 min at 4 °C, the supernatants were transferred to vials for later LC-MS analysis.

Metabolomics Analysis. LC separation was achieved in a Vanquish UHPLC system (Thermo Fisher Scientific) equipped with a hydrophilic interaction chromatography column (Xbridge BEH Amide XP column, 130Å, 2.5 µm, 2.1 mm × 150 mm, Waters, Milford, MA). Mobile phases were 20 mM ammonium acetate and 20 mM ammonium hydroxide in 95:5 water:acetonitrile (pH 9.4) as eluent A and acetonitrile as eluent B. Column temperature set at 25 °C, and a flow rate was 150 µL min^{-1}. The gradient was as follows: 90% B at 0 min, 90% B at 0.5 min, 75% B at 1.5 min, 75% B at 5.5 min, 70% B at 6.5 min, 70% B at 7.5 min, 50% B at 8.5 min, 50% B at 10.5 min, 25% B at 11.5 min, 25% B at 12.5 min, %0 B at 14.5 min, 0% B at 20 min, 90% B at 20.5 min, and 90% B at 26 min. The total run time was 26 min at a flow rate of 150 µL min^{-1} (79). The injection volumes were 2 and 10 µL for extracellular and intracellular metabolite samples, respectively. LC separation of folates species was on a reversed-phase column (Agilent InfinityLab Poroshell 120 Bonus-RP 2.7 µm, 2.1 × 150Â mm) with 10 mM ammonium acetate and 0.1% vol of acetic acid in 95:5 water:acetonitrile as eluent A and acetonitrile as eluent B. Gradient conditions were 2% B at 0 min, 98% B at 20 min, 98% B at 25min, 2% B at 26 min, 2% at 35 min. The flow rate was 200 µL min^{-1}, and the column temperature was 25 °C. The injection volume was 20 µL.

For mass spectrometry, the above-described LC systems were interfaced with Q-Exactive Plus Hybrid Quadrupole-Orbitrap Mass Spectrometer (Thermo Fisher Scientific). The mass spectra were collected in positive mode scanning mass-to-charge (m/z) ratio range between 60 to 900, and negative mode scanning m/z 60 to 200 and m/z 200 to 2,000 at a resolution of 140,000 at m/z 200, with automatic gain control (AGC) target 3e6, and maximum injection time (IT) of 500 ms. For folate species, mass spectra were collected only in positive scanning m/z 442 to 476 at a resolution of 35,000 at m/z 200 and a maximum IT of 200 ms. The authenticated standards including more than 400 metabolites were applied to verify the retention time (80). For MS/MS analysis, full MS/dd-MS2 mode was used. Full MS was in positive scanning m/z 100 to 1,000 at a resolution of

140,000 at *m/z* 200, and a maximum IT of 120 ms. MS/MS scanning was with a resolution of 70,000 at *m/z* 200, a maximum IT of 100 ms, an isolation window of 2 *m/z*, minimum AGC 1.0e3, and normalized collision energy (NCE) of 30 with an inclusion list of targeted metabolites.

Data were collected using Thermo Scientific Xcalibur data acquisition and interpretation software (version 4.2.27) and Q-Exactive MS series Tune interface (version 2.11). Data analysis was processed using the Maven software package (81). Metabolite identification was based on the exact *m/z* with mass error less than 10 ppm and a retention time difference smaller than 1 min to the authenticated standards (79). The abundance of each metabolite was reported after integrating the top peak area in extracted ion chromatogram and normalized to the protein concentration in culture.

Proteome Extraction and Sample Preparation. After a three-day experiment, cell pellets from 40-mL culture suspensions were collected by centrifuging at 7,547 × g for 20 min using Sorvall ST 8 centrifuge (Thermo Fisher Scientific). The proteome was extracted using the established protocol (16). Cell pellets were resuspended in 0.5-mL lysis buffer consisted of 100 mM Tris, 8 M urea, 35 mM sodium dodecyl sulfate, protease inhibitor (Thermo Fisher Scientific), and benzonase nuclease (MilliporeSigma), and sonicated using the point sonicator for 10 s on the ice bath followed by rotation at 4 °C for 30 min. The proteins present in the supernatant were collected by centrifuging at 16,000 × g for 15 min at 4 °C. The proteins were reduced, alkylated, and digested following the established procedures (16). Following the digestion, the peptides eluted from carboxylate-modified magnetic beads were dried by vacuum centrifugation and reconstituted in 5% formic acid before analysis by LC-MS/MS (Liquid chromatography–tandem mass spectrometry).

Proteomics Analysis. Peptide samples were separated on a 75 μm ID, 25 cm C18 column packed with 1.9 μm C18 particles (Dr. Maisch GmbH HPLC) using a 140-min gradient of increasing acetonitrile concentration and injected into a Thermo Orbitrap-Fusion Lumos Tribrid mass spectrometer. MS/MS spectra were acquired using Data Dependent Acquisition (DDA) mode.

MS/MS database searching was performed using MaxQuant (1.6.10.43) against the *S. ovata* DSM 2662 reference proteome from Uniprot (UP000015521, 5045 entries). The domain annotation and functional prediction of proteins were obtained from UniParc. The KEGG orthology (KO) assignment based on the amino acid sequence of the protein was performed using BlastKOALA which was used for pathway analysis against KEGG database (82).

Statistical analysis of MaxQuant label-free quantitation data was performed with the artMS Bioconductor package which performs the relative quantification of protein abundance using the MSstats Bioconductor package (default parameters). Intensities were normalized across samples by median-centering the log2-transformed MS1 intensity distributions. The abundance of proteins missing from one condition but found in more than two biological replicates of the other condition for any given comparison was estimated by imputing intensity values from the lowest observed MS1-intensity across samples.

Data, Materials, and Software Availability. The metabolomic and proteomic data reported in this study are available in the Datasets S1 and S2. All other data are included in the manuscript and/or supporting information.

ACKNOWLEDGMENTS. C.L. acknowledges the support from NIH (R35GM138241), Sloan Research Fellowship from Alfred P. Sloan Foundation, and the Jeffery and Helo Zink Endowed Professional Development Term Chair.

Author affiliations: [a]Department of Chemistry and Biochemistry, University of California, Los Angeles, CA 90095; [b]Department of Chemical and Biomolecular Engineering, University of California, Los Angeles, CA 90095; [c]Department of Biological Chemistry, University of California, Los Angeles, CA 90095; and [d]California NanoSystems Institute, University of California, Los Angeles, CA 90095

1. H. Chen, F. Dong, S. D. Minteer, The progress and outlook of bioelectrocatalysis for the production of chemicals, fuels and materials. *Nat. Catal.* **3**, 225–244 (2020).
2. D. K. Dogutan, D. G. Nocera, Artificial photosynthesis at efficiencies greatly exceeding that of natural photosynthesis. *Acc. Chem. Res.* **52**, 3143–3148 (2019).
3. N. Kornienko, J. Z. Zhang, K. K. Sakimoto, P. Yang, E. Reisner, Interfacing nature's catalytic machinery with synthetic materials for semi-artificial photosynthesis. *Nat. Nanotechnol.* **13**, 890–899 (2018).
4. O. Adesina, I. A. Anzai, J. L. Avalos, B. Barstow, Embracing biological solutions to the sustainable energy challenge. *Chem* **2**, 20–51 (2017).
5. T. Zhang, More efficient together. *Science* **350**, 738–739 (2015).
6. K. P. Nevin, T. L. Woodard, A. E. Franks, Z. M. Summers, D. R. Lovley, Microbial electrosynthesis: Feeding microbes electricity to convert carbon dioxide and water to multicarbon extracellular organic compounds. *mBio* **1**, e00103–e00110 (2010).
7. C. Liu, B. C. Colón, M. Ziesack, P. A. Silver, D. G. Nocera, Water splitting–biosynthetic system with CO_2 reduction efficiencies exceeding photosynthesis. *Science* **352**, 1210–1213 (2016).
8. R. S. Sherbo, P. A. Silver, D. G. Nocera, Riboflavin synthesis from gaseous nitrogen and carbon dioxide by a hybrid inorganic-biological system. *Proc. Natl. Acad. Sci. U.S.A.* **119**, e2210538119 (2022).
9. H. Li *et al.*, Integrated electromicrobial conversion of CO_2 to higher alcohols. *Science* **335**, 1596–1596 (2012).
10. B. E. Logan, R. Rossi, A. Ragab, P. E. Saikaly, Electroactive microorganisms in bioelectrochemical systems. *Nat. Rev. Microbiol.* **17**, 307–319 (2019).
11. B. E. Logan, K. Rabaey, Conversion of wastes into bioelectricity and chemicals by using microbial electrochemical technologies. *Science* **337**, 686–690 (2012).
12. K. Rabaey, R. A. Rozendal, Microbial electrosynthesis-revisiting the electrical route for microbial production. *Nat. Rev. Microbiol.* **8**, 706–716 (2010).
13. H. Chen *et al.*, Fundamentals, applications, and future directions of bioelectrocatalysis. *Chem. Rev.* **120**, 12903–12993 (2020).
14. C. Liu, K. K. Sakimoto, B. C. Colón, P. A. Silver, D. G. Nocera, Ambient nitrogen reduction cycle using a hybrid inorganic–biological system. *Proc. Natl. Acad. Sci. U.S.A.* **114**, 6450–6455 (2017).
15. C. Liu *et al.*, Nanowire–bacteria hybrids for unassisted solar carbon dioxide fixation to value-added chemicals. *Nano Lett.* **15**, 3634–3639 (2015).
16. X. Guan *et al.*, Maximizing light-driven CO_2 and N_2 fixation efficiency in quantum dot–bacteria hybrids. *Nat. Catal.* **5**, 1019–1029 (2022).
17. K. K. Sakimoto, A. B. Wong, P. Yang, Self-photosensitization of nonphotosynthetic bacteria for solar-to-chemical production. *Science* **351**, 74–77 (2016).
18. Y. He *et al.*, Photosynthesis of acetate by *Sporomusa ovata*–CdS biohybrid system. *ACS Appl. Mater. Inter.* **14**, 23364–23374 (2022).
19. J. Ye *et al.*, Solar-driven methanogenesis with ultrahigh selectivity by turning down H_2 production at biotic-abiotic interface. *Nat. Commun.* **13**, 6612 (2022).
20. K. Kuruvinashetti, N. Kornienko, Pushing the methodological envelope in understanding the photo/electrosynthetic materials-microorganism interface. *iScience* **24**, 103049 (2021).
21. P. Li, S. Kim, B. Tian, Nanoenabled trainable systems: From biointerfaces to biomimetics. *ACS Nano* **16**, 19651–19664 (2022).
22. X. Meng, L. Liu, X. Chen, Bacterial photosynthesis: State-of-the-art in light-driven carbon fixation in engineered bacteria. *Curr. Opin. Microbiol.* **69**, 102174 (2022).
23. J. Deutzmann, S. F. Kracke, W. Gu, A. M. Spormann, Microbial electrosynthesis of acetate powered by intermittent electricity. *Environ. Sci. Technol.* **56**, 16073–16081 (2022).
24. S. A. Patil *et al.*, Selective enrichment establishes a stable performing community for microbial electrosynthesis of acetate from CO_2. *Environ. Sci. Technol.* **49**, 8833–8843 (2015).
25. T. Krieg, A. Sydow, S. Faust, I. Huth, D. Holtmann, CO_2 to terpenes: Autotrophic and electroautotrophic α-humulene production with *Cupriavidus necator*. *Angew. Chem. Int. Ed.* **57**, 1879–1882 (2018).
26. J. P. Torella *et al.*, Efficient solar-to-fuels production from a hybrid microbial–water-splitting catalyst system. *Proc. Natl. Acad. Sci. U.S.A.* **112**, 2337–2342 (2015).
27. S. Lu, X. Guan, C. Liu, Electricity-powered artificial root nodule. *Nat. Commun.* **11**, 1505 (2020).
28. E. M. Nichols *et al.*, Hybrid bioinorganic approach to solar-to-chemical conversion. *Proc. Natl. Acad. Sci. U.S.A.* **112**, 11461–11466 (2015).
29. A. R. Rowe *et al.*, Methane-linked mechanisms of electron uptake from cathodes by *Methanosarcina barkeri*. *mBio* **10**, e02448–e02418 (2019).
30. J. Kim, S. Cestellos-Blanco, Y. Shen, R. Cai, P. Yang, Enhancing biohybrid CO_2 to multicarbon reduction via adapted whole-cell catalysts. *Nano Lett.* **22**, 5503–5509 (2022).
31. R. M. Rodrigues *et al.*, Perfluorocarbon nanoemulsion promotes the delivery of reducing equivalents for electricity-driven microbial CO_2 reduction. *Nat. Catal.* **2**, 407–414 (2019).
32. N. Aryal, P.-L. Tremblay, D. M. Lizak, T. Zhang, Performance of different *Sporomusa* species for the microbial electrosynthesis of acetate from carbon dioxide. *Bioresour. Technol.* **233**, 184–190 (2017).
33. S. Cestellos-Blanco *et al.*, Photosynthetic biohybrid coculture for tandem and tunable CO_2 and N_2 fixation. *Proc. Natl. Acad. Sci. U.S.A.* **119**, e2122364119 (2022).
34. Y. Su *et al.*, Close-packed nanowire-bacteria hybrids for efficient solar-driven CO_2 fixation. *Joule* **4**, 800–811 (2020).
35. R. Zhang *et al.*, Proteomic and metabolic elucidation of solar-powered biomanufacturing by bio-abiotic hybrid system. *Chem* **6**, 234–249 (2020).
36. S. W. Ragsdale, E. Pierce, Acetogenesis and the Wood-Ljungdahl pathway of CO_2 fixation. *Biochim. Biophys. Acta. Proteins. Proteom.* **1784**, 1873–1898 (2008).
37. N. Aryal *et al.*, Increased carbon dioxide reduction to acetate in a microbial electrosynthesis reactor with a reduced graphene oxide-coated copper foam composite cathode. *Bioelectrochemistry* **128**, 83–93 (2019).
38. N. Jiang, B. You, M. Sheng, Y. Sun, Electrodeposited cobalt-phosphorous-derived films as competent bifunctional catalysts for overall water splitting. *Angew. Chem.* **127**, 6349–6352 (2015).
39. B. Möller, R. Oßmer, B. H. Howard, G. Gottschalk, H. Hippe, *Sporomusa*, a new genus of gram-negative anaerobic bacteria including *Sporomusa sphaeroides* spec. nov. and *Sporomusa ovata* spec. nov. *Arch. Microbiol.* **139**, 388–396 (1984).
40. N. Uría, X. Muñoz Berbel, O. Sánchez, F. X. Muñoz, J. Mas, Transient storage of electrical charge in biofilms of *Shewanella oneidensis* MR-1 growing in a microbial fuel cell. *Environ. Sci. Technol.* **45**, 10250–10256 (2011).
41. R. Milo, What is the total number of protein molecules per cell volume? A call to rethink some published values *Bioessays* **35**, 1050–1055 (2013).
42. M. Y. El-Naggar *et al.*, Electrical transport along bacterial nanowires from *Shewanella oneidensis* MR-1. *Proc. Natl. Acad. Sci. U.S.A.* **107**, 18127–18131 (2010).
43. Y. Xie *et al.*, *Pseudomonas* sp. strain 273 degrades fluorinated alkanes. *Environ. Sci. Technol.* **54**, 14994–15003 (2020).

44. D. E. Canfield, E. Kristensen, B. Thamdrup, "Thermodynamics and microbial metabolism" in *Advances in Marine Biology* (Elsevier, 2005), **vol. 48**, chap. 3, pp. 65–94.
45. A. Grimalt-Alemany, C. Etler, K. Asimakopoulos, I. V. Skiadas, H. N. Gavala, ORP control for boosting ethanol productivity in gas fermentation systems and dynamics of redox cofactor NADH/NAD^+ under oxidative stress *J. CO2 Util.* **50**, 101589 (2021).
46. S. J. Berrıos-Rivera, G. N. Bennett, K.-Y. San, The effect of increasing NADH availability on the redistribution of metabolic fluxes in *Escherichia coli* chemostat cultures. *Metab. Eng.* **4**, 230–237 (2002).
47. S. Spahn, K. Brandt, V. Müller, A low phosphorylation potential in the acetogen *Acetobacterium woodii* reflects its lifestyle at the thermodynamic edge of life. *Arch. Microbiol.* **197**, 745–751 (2015).
48. M. H. Buckstein, J. He, H. Rubin, Characterization of nucleotide pools as a function of physiological state in *Escherichia coli*. *J. Bacteriol.* **190**, 718–726 (2008).
49. K. R. Sowers, R. P. Gunsalus, Halotolerance in *Methanosarcina* spp.: Role of N-acetyl-lysine, glutamate, glycine betaine, and K^+ as compatible solutes for osmotic adaptation *Appl. Environ. Microbiol.* **61**, 4382–4388 (1995).
50. A. Poehlein, G. Gottschalk, R. Daniel, First insights into the genome of the Gram-negative, endospore-forming organism *Sporomusa ovata* strain H1 DSM 2662. *Genome Announc.* **1**, e00734–00713 (2013).
51. J. Madjarov, R. Soares, C. M. Paquete, R. O. Louro, *Sporomusa ovata* as catalyst for bioelectrochemical carbon dioxide reduction: A review across disciplines from microbiology to process engineering. *Front. Microbiol.* **13**, 913311 (2022).
52. N. Chu *et al.*, Microbial electrosynthesis for producing medium chain fatty acids. *Engineering* **16**, 141–153 (2021).
53. D. Litty, V. Müller, ATP synthesis in an ancient ATP synthase at low driving forces. *Proc. Natl. Acad. Sci. U.S.A.* **119**, e2201921119 (2022).
54. P.-L. Tremblay, T. Zhang, S. A. Dar, C. Leang, D. R. Lovley, The Rnf complex of *Clostridium ljungdahlii* is a proton-translocating ferredoxin: NAD^+ oxidoreductase essential for autotrophic growth *mBio* **4**, e00406–00412 (2013).
55. F. P. Rosenbaum, V. Müller, Energy conservation under extreme energy limitation: The role of cytochromes and quinones in acetogenic bacteria. *Extremophiles* **25**, 413–424 (2021).
56. F. Kremp, J. Roth, V. Müller, A third way of energy conservation in acetogenic bacteria. *Microbiol. Spectr.* **10**, e0138522 (2022).
57. D. White, J. T. Drummond, C. Fuqua, *The Physiology and Biochemistry of Prokaryotes* (Oxford University Press, 2012), pp. 111–141.
58. A. G. Fast, E. T. Papoutsakis, Stoichiometric and energetic analyses of non-photosynthetic CO_2-fixation pathways to support synthetic biology strategies for production of fuels and chemicals. *Curr. Opin. Chem. Eng.* **1**, 380–395 (2012).
59. K. Schuchmann, V. Müller, Autotrophy at the thermodynamic limit of life: A model for energy conservation in acetogenic bacteria. *Nat. Rev. Microbiol.* **12**, 809–821 (2014).
60. F. Mayer, V. Müller, Adaptations of anaerobic archaea to life under extreme energy limitation. *FEMS Microbiol. Rev.* **38**, 449–472 (2014).
61. E. Marsili *et al.*, *Shewanella* secretes flavins that mediate extracellular electron transfer. *Proc. Natl. Acad. Sci. U.S.A.* **105**, 3968–3973 (2008).
62. S. L. Tan, R. D. Webster, Electrochemically induced chemically reversible proton-coupled electron transfer reactions of riboflavin (vitamin B_2). *J. Am. Chem. Soc.* **134**, 5954–5964 (2012).
63. E. C. Smith, D. E. Metzler, The photochemical degradation of riboflavin. *J. Am. Chem. Soc.* **85**, 3285–3288 (1963).
64. F. Kracke, I. Vassilev, J. O. Krömer, Microbial electron transport and energy conservation–the foundation for optimizing bioelectrochemical systems. *Front. Microbiol.* **6**, 575 (2015).
65. A. Gemünde, B. Lai, L. Pause, J. Krömer, D. Holtmann, Redox mediators in microbial electrochemical systems. *ChemElectroChem* **9**, e202200216 (2022).
66. F. Kracke, B. Virdis, P. V. Bernhardt, K. Rabaey, J. O. Krömer, Redox dependent metabolic shift in *Clostridium autoethanogenum* by extracellular electron supply. *Biotechnol. Biofuels* **9**, 249 (2016).
67. A. Okamoto, K. Hashimoto, K. H. Nealson, Flavin redox bifurcation as a mechanism for controlling the direction of electron flow during extracellular electron transfer. *Angew. Chem. Int. Ed.* **53**, 10988–10991 (2014).
68. F. Jiménez Otero, D. K. Newman, L. M. Tender, Pyocyanin-dependent electrochemical inhibition of *Pseudomonas aeruginosa* biofilms is synergistic with antibiotic treatment. *mBio*, e00702–00723 (2023).
69. A. Pradet, P. Raymond, Adenine nucleotide ratios and adenylate energy charge in energy metabolism. *Annu. Rev. Plant. Biol.* **34**, 199–224 (1983).
70. R. Moscoviz, J. Toledo-Alarcón, E. Trably, N. Bernet, Electro-fermentation: How to drive fermentation using electrochemical systems. *Trends Biotechnol.* **34**, 856–865 (2016).
71. G. Rao, R. Mutharasan, Altered electron flow in continuous cultures of *Clostridium acetobutylicum* induced by viologen dyes. *Appl. Environ. Microbiol.* **53**, 1232–1235 (1987).
72. T. S. Kim, B. H. Kim, Electron flow shift in *Clostridium acetobutylicum* fermentation by electrochemically introduced reducing equivalent. *Biotechnol. Lett.* **10**, 123–128 (1988).
73. K. P. Nevin *et al.*, Electrosynthesis of organic compounds from carbon dioxide is catalyzed by a diversity of acetogenic microorganisms. *Appl. Environ. Microbiol.* **77**, 2882–2886 (2011).
74. Q. Wang, S. Kalathil, C. Pornrungroj, C. D. Sahm, E. Reisner, Bacteria–photocatalyst sheet for sustainable carbon dioxide utilization. *Nat. Catal.* **5**, 633–641 (2022).
75. F. E. Loffler, R. A. Sanford, J. M. Tiedje, Initial characterization of a reductive dehalogenase from *Desulfitobacterium chlororespirans* Co23. *Appl. Environ. Microbiol.* **62**, 3809–3813 (1996).
76. J. He, K. M. Ritalahti, K.-L. Yang, S. S. Koenigsberg, F. E. Löffler, Detoxification of vinyl chloride to ethene coupled to growth of an anaerobic bacterium. *Nature* **424**, 62–65 (2003).
77. R. Sander, Compilation of Henry's law constants (version 4.0) for water as solvent. *Atmos. Chem. Phys.* **15**, 4399–4981 (2015).
78. A. F. Schober *et al.*, A two-enzyme adaptive unit within bacterial folate metabolism. *Cell Rep.* **27**, 3359–3370.e3357 (2019).
79. L. Wang *et al.*, Peak annotation and verification engine for untargeted LC–MS metabolomics. *Anal. Chem.* **91**, 1838–1846 (2018).
80. J. O. Park *et al.*, Synergistic substrate cofeeding stimulates reductive metabolism. *Nat. Metab.* **1**, 643–651 (2019).
81. M. F. Clasquin, E. Melamud, J. D. Rabinowitz, LC-MS data processing with MAVEN: A metabolomic analysis and visualization engine. *Curr. Protoc. Bioinf.* **37**, 14.11.11–14.11.23 (2012).
82. M. Kanehisa, Y. Sato, K. Morishima, BlastKOALA and GhostKOALA: KEGG tools for functional characterization of genome and metagenome sequences. *J. Mol. Biol.* **428**, 726–731 (2016).